EVOLUTION OF THE ELECTRON YIELD CURVES OF INSULATORS AS A FUNCTION OF IMPINGING ELECTRON FLUENCE AND ENERGY

J.R. Dennison and Alec Sim
Physics Department, Utah State University
SER 250 UMC 4415, Logan, UT, USA 84322-4415
Phone: 435.797.2936, Fax: 435.797.2492, JR.Dennison@usu.edu

Clint Thomson
Health Management Focus Group, ATK Thiokol
P.O. Box 707, M/S 245C, Brigham City, UT, USA 84302-0707
Phone: 435.863.3562, Fax: 435.863.2443, Clint.Thomson@atk.com

Abstract

Electron emission and concomitant charge accumulation near the surface of insulators is central to understanding spacecraft charging. We present a study of changes in electron emission yields as a result of internal charge build up due to electron dose. Evolution of total, backscattered and secondary yield results over a broad range of incident energies are presented for two representative insulators, Kapton™ and Al_2O_3. Reliable yield curves for un-charged insulators are measured and quantifiable changes in yields are observed due to <100 fC/mm^2 fluences. We find excellent agreement with a phenomenological argument based on insulator charging predicted by the yield curve; this includes a decrease in the rate of change of the yield as incident energies approach the crossover energies and as accumulated internal charge reduces the landing energy to asymptotically approach a steady state surface charge and unity yield. We also find that the exponential decay of yield curves with fluence exhibit an energy dependant decay constant, $\alpha(E)$. Finally, we discuss physics based models for this energy dependence. To understand fluence and energy dependence of these charging processes requires knowledge of how charge is deposited within the insulator, the mechanisms for charge trapping and transport within the insulator, and how the profile of trapped charge affects the transport and emission of charges from insulators.

Introduction

The central theme of the 9th Spacecraft Charging Conference has been how spacecraft interact with the plasma environment to cause charging. Spacecraft accumulate charge and adopt potentials in response to interactions with the plasma environment. Key parameters in modeling spacecraft charging are the electron emission properties of insulating materials. This determines how much charge will accumulate in key spacecraft components in response to incident electron, ion and photon fluxes. Due to their high mobility, incident electrons play a more significant role in spacecraft charging and are therefore the focus of this presentation. Electrons generally move faster than spacecraft while ions do not. Thus, even if electron and ion densities are equal, differential charging can occur on spacecraft surfaces. We approach spacecraft charging from the materials physics point of view, studying how charge is accumulated and concentrating on length scales of microns rather than meters.

In this paper, we present a study of the changes in electron-induced electron yields and emission spectra that result from the build up of internal charge distributions due to incident and emitted electron fluxes. Specifically, we will look at how charge build-up in insulating materials affects these fluxes. First, measurements of reliable yield curves for uncharged insulators are shown. Evolution of total, backscattered and secondary yield results over a broad range of incident energies in response to accumulated charge are presented for representative insulators. Quantifiable changes in yields are observed due to <100 fC/mm^2 fluences. Next, we present measurements of various changes to the electron emission spectra that result from charge accumulation. Finally, decay curves are presented that show the evolution of the electron yield for specific incident electron energies as a function of incident electron fluence.

Electron Emission From Conductors and Insulators

The electron emission properties of conductors are relatively easy to measure [1,2]. However, yield measurements on dielectrics are more difficult because the materials charge [3,4]. Surface potentials resulting from the accumulated charge can affect yields by altering incident (or landing) energies or by affecting the escape energies of secondary and

backscattered electrons. Accumulated charge in insulators interacts with incident charged particles through Coulomb interactions and affects electron emission in all three stages of emission models discussed below. We present both qualitative and quantitative data showing these effects and attempt to relate them to existing semi-empirical theory of electron emission [3-5].
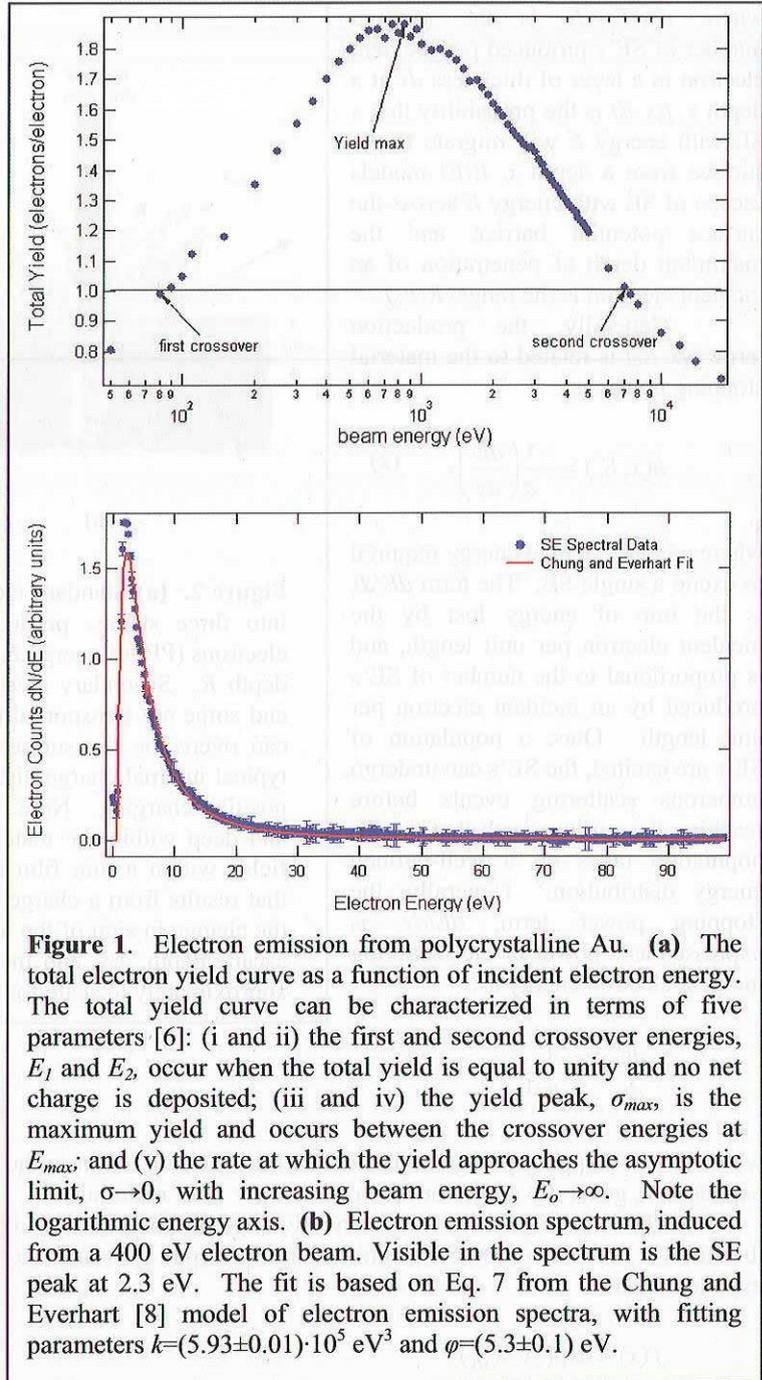
Models of Electron Yields

We begin by reviewing the basic physics of electron emission. The total yield, σ, is the ratio of emitted flux to incident flux. By convention, the secondary electron (SE) yield, $\delta(E_o)$, is the ratio for emitted electrons with energy <50 eV and the backscattered electron (BSE) yield, $\eta(E_o)$, is the ratio for emitted electrons with energy >50 eV. An electron yield curve shows the yield as a function of incident electron energy (see Figure 1a). The total yield curve can be characterized in terms of five parameters [6]: (i and ii) the first and second crossover energies, E_1 and E_2, occur when the total yield is equal to unity and no net charge is deposited; (iii and iv) the yield peak, σ_{max}, is the maximum yield and occurs between the crossover energies at E_{max} (The maximum yield is typically found between $200<E_{max}<1000$ eV.); and (v) the rate at which the yield approaches the asymptotic limit, $\sigma\rightarrow0$, with increasing beam energy, $E_o\rightarrow\infty$. Measured yield curves are presented later and are shown in Figures 1, 4 and 5.

Standard models of electron emission divide the process into three stages (see Figure 2a):

1) *Production:* Primary electrons deposit energy as they interact with the target material and energize material electrons. The key parameter is the inelastic mean free path of the incident electron, λ_{PE}. Most SE are

Figure 1. Electron emission from polycrystalline Au. **(a)** The total electron yield curve as a function of incident electron energy. The total yield curve can be characterized in terms of five parameters [6]: (i and ii) the first and second crossover energies, E_1 and E_2, occur when the total yield is equal to unity and no net charge is deposited; (iii and iv) the yield peak, σ_{max}, is the maximum yield and occurs between the crossover energies at E_{max}; and (v) the rate at which the yield approaches the asymptotic limit, $\sigma\rightarrow0$, with increasing beam energy, $E_o\rightarrow\infty$. Note the logarithmic energy axis. **(b)** Electron emission spectrum, induced from a 400 eV electron beam. Visible in the spectrum is the SE peak at 2.3 eV. The fit is based on Eq. 7 from the Chung and Everhart [8] model of electron emission spectra, with fitting parameters $k=(5.93\pm0.01)\cdot10^5$ eV^3 and $\varphi=(5.3\pm0.1)$ eV.

produced near the maximum range of penetration, R, which increases with increasing incident energy and is usually much greater than the inelastic mean free path of the lower energy secondary electron, λ_{SE}.

2) *Secondary Electron Transport:* The probability that SE produced at a depth x reaches the surface decays exponentially with depth due to energy losses through inelastic scattering. The key parameter is λ_{SE}, which is typically much less than λ_{PE} for the higher energy incident electrons.

3) *Emission:* Those SE that make it to the surface and can cross the surface potential barrier are emitted.

This process is described by an equation for the secondary yield as a function of incident energy [3,7] as

$$\delta(E_O) = \int_0^{R(E_o)} n(x;E_o)\cdot f(x;E)\cdot B(E)\,dx \qquad (1)$$

where $n(x;E_o)\cdot dx$ is the average number of SE's produced per incident electron in a layer of thickness dx at a depth x, $f(x;E)$ is the probability that a SE with energy E will migrate to the surface from a depth x, $B(E)$ models escape of SE with energy E across the surface potential barrier, and the maximum depth of penetration of an incident electron is the range, $R(E_o)$.

Generally, the production term, $n(x;E_0)$ is related to the material stopping power as:

$$n(x, E_0) = -\frac{1}{\varepsilon}\left(\frac{dE}{dx}\right), \quad (2)$$

where ε is the average energy required to excite a single SE. The term dE/dx is the rate of energy lost by the incident electron per unit length, and is proportional to the number of SE's produced by an incident electron per unit length. Once a population of SE's are excited, the SE's can undergo numerous scattering events before reaching the surface, such that the SE population takes on a well-defined energy distribution. Generally, the stopping power term, dE/dx, is expressed as a power of the scattering incident electron energy as:

Figure 2. **(a)** Standard models of electron emission divide the process into three stages: production, SE transport and escape. Primary electrons (PE) of energy E_o impinge on the surface and penetrate up to a depth R. Secondary electrons (SE) are produced within the material and some are transported to the surface. A fraction of these electrons can overcome the surface barrier and escape. **(b)** Schematic of a typical internal charge distribution for $E_1 < E_o < E_2$ with $\sigma > 1$ and overall positive charging. Note the negative charge regions near the surface and deep within the material. **(c)** Schematic of the internal electric fields within a thin film insulator with grounded conductive backing that results from a charge distribution such as that shown in (b). Note the change in sign of the internal electric field. The secondary electron escape depth, λ_{SE}, and incident electron range, $R(Eo)$, are also shown approximately to scale for typical incident energies in this regime.

$$-\frac{dE}{dx} = \frac{A}{E_o^{n-1}} \quad (3)$$

where A is a stopping power coefficient of the material, and n is the stopping power exponent. The stopping power exponent, n, generally ranges between 1 and 2 for most materials.
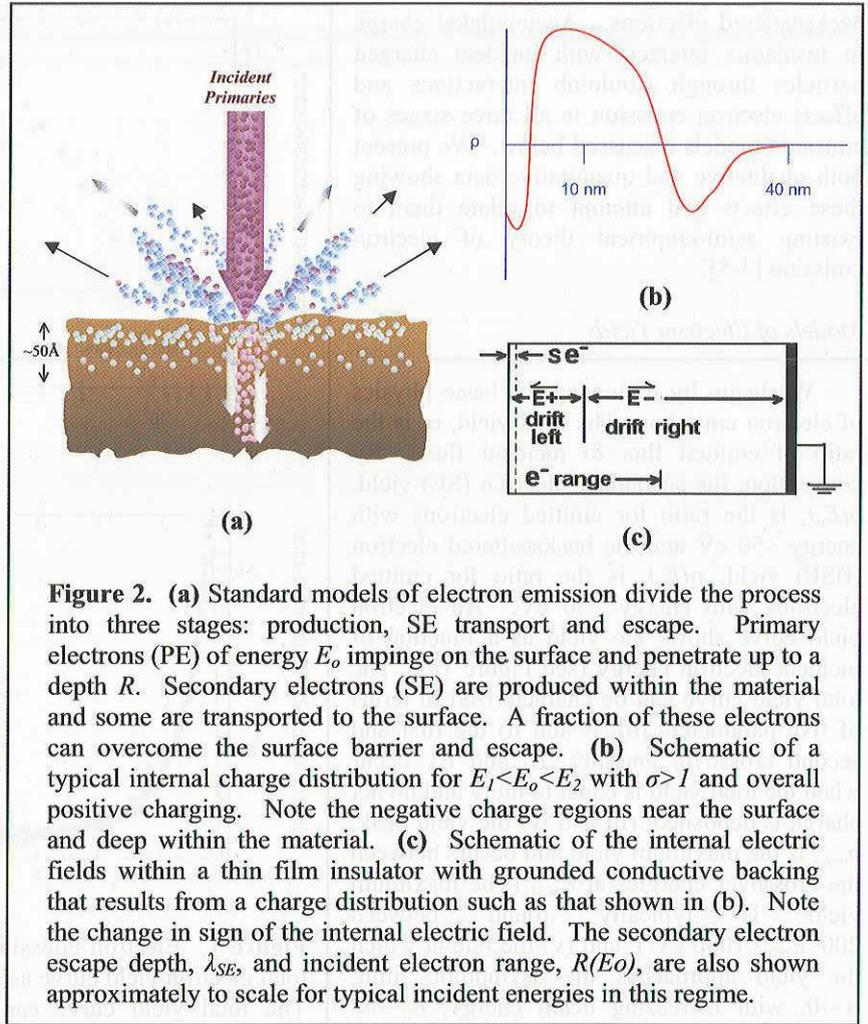
The term, $f(x)$ in Eq. 1 contains SE transport components, and represents the probability an SE will diffuse to the surface. To first order, SE migration from a depth x towards the surface can be approximated by a diffusion-like exponential law:

$$f(x) \approx \exp(-x/\lambda_{SE}), \quad (4)$$

where λ_{SE} is the mean SE escape depth that incorporates trapping probabilities, inelastic, and elastic scatterings. The escape term $B(E)$ is a material-dependent term that represents the SE escape probability over surface energy barriers and is usually approximated as an energy-independent probability coefficient that ranges between 0 and 1 (0: no escape, 1: escape) [7]. For unbiased conductors, B has been related to the work function [8], and for uncharged insulators, it has been related to the bandgap energy and electron affinity[9]. For biased conductors or charged insulators, the surface barrier has an additional contribution related to eV_s, where V_s is the surface potential [10].

By combining Eqs. 1, 2 and 4, the general expression for the SE yield can be written as:

$$\delta(E_o) = -\frac{B}{\varepsilon} \int_0^{R(E_o)} \frac{dE}{dx} \cdot e^{-x/\lambda_{SE}} \, dx \quad (5)$$

Figure 3. Illustration of modified SE spectra resulting from surface potentials due to conductor bias or insulator surface charging. **(a)** Schematic representation of the effect of surface potential on normally emitted SE. **(Left)** SE emission from unbiased surface. **(Center)** SE are given a boost in kinetic energy as they leave a negatively biased surface. **(Right)** The electric field from the positive charge region re-attracts the lowest energy SE emitted from the surface, thereby establishing a shallow negative surface charge region. **(b)** Negative surface charging causes escaping SE to gain kinetic energy, thus pushing the higher-energy portion of the SE spectrum (represented by the shaded area) to energies beyond 50 eV. **(c)** Positive surface charging prohibits the escape of lower-energy SE's, thus suppressing the lower-energy portion of the SE spectrum (represented by the shaded area). **(d)** The fraction of SE allowed to escape the surface as a function of evolving positive surface potential V_s in the positive charging region where $E_1 < E_0 < E_2$. The curve is calculated using Eq. 12.. Between the crossover energies, typical fractional SE yields for insulators approach values of 0.2-0.6, corresponding to positive surface potentials of 4-10 V.
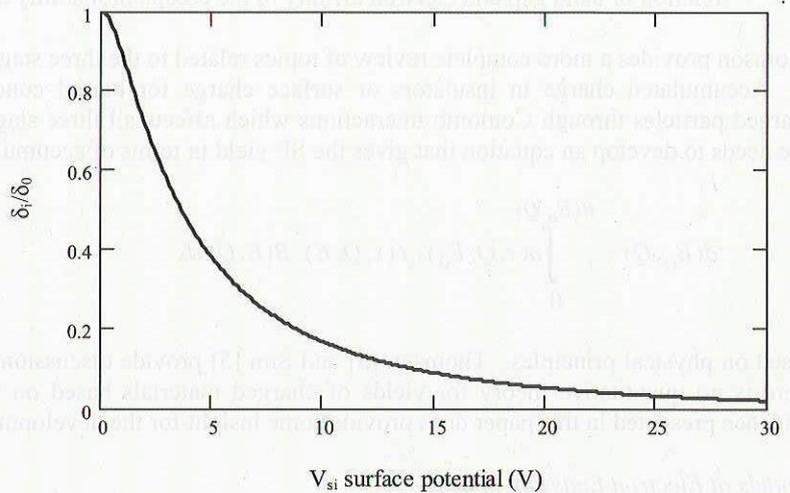

(b)

(c)

(d)

(a)
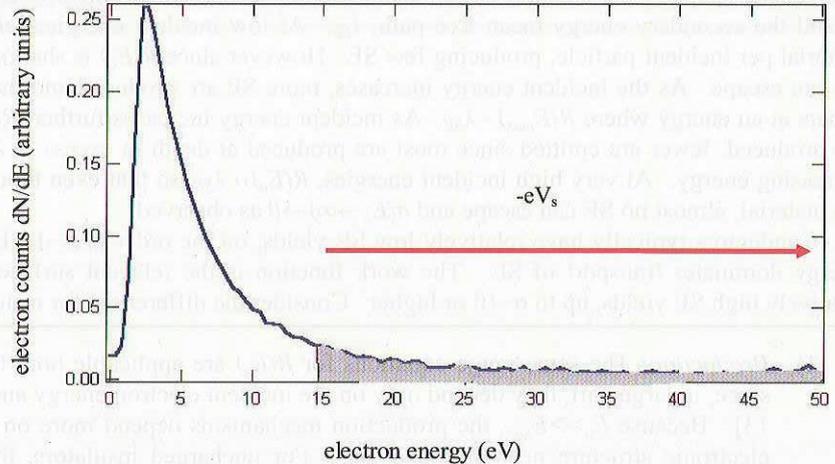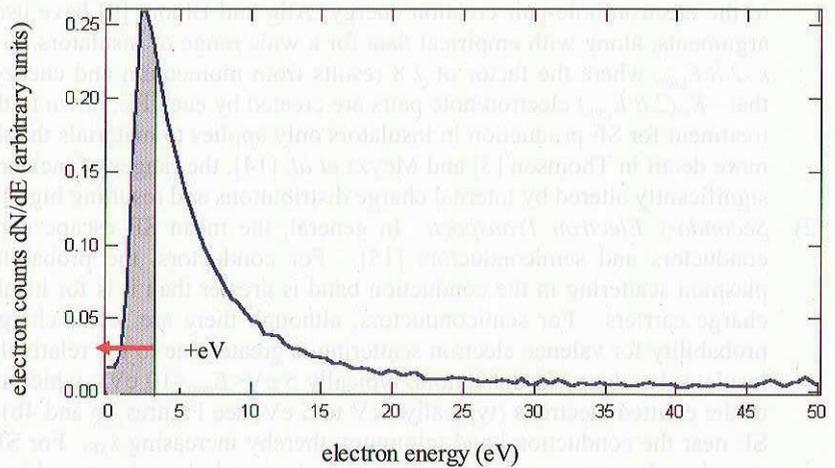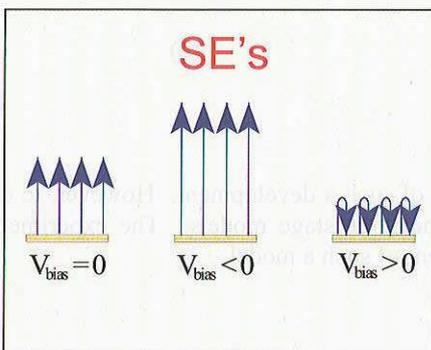
The general shape of the yield curve can be understood as a competition between the incident energy penetration depth, R, and the secondary energy mean free path, λ_{SE}. At low incident energies relatively little energy is imparted to the material per incident particle, producing few SE. However since $R(E_o)$ is shallow—on the order of λ_{SE}—many of these SE can escape. As the incident energy increases, more SE are produced and the yield increases. The maximum yield occurs at an energy where $R(E_{max}) \sim \lambda_{SE}$. As incident energy increases further, $R(E_o)$ exceeds λ_{SE}; even though more SE are produced, fewer emitted since most are produced at depth in excess of λ_{SE}. Thus, the yield begins to fall with increasing energy. At very high incident energies, $R(E_o) \gg \lambda_{SE}$, so that even though many SE are produced deep within the material, almost no SE can escape and $\sigma(E_o \rightarrow \infty) \rightarrow 0$ as observed.

Conductors typically have relatively low SE yields, on the order of $\sigma \sim 1$. Electron-electron scatter near the Fermi energy dominates transport of SE. The work function is the relevant surface barrier. By contrast, insulators have relatively high SE yields, up to $\sigma \sim 10$ or higher. Consider the differences for insulators in each stage:

1) *Production:* The same range equations for $R(E_o)$ are applicable both to conductors and uncharged insulators since, in large part, they depend only on the incident electron energy and macroscopic density of materials [11-13]. Because $E_o \gg E_{gap}$, the production mechanisms depend more on electron density than on details of the electronic structure near the band gap. For uncharged insulators, the primary difference between the SE production mechanisms, in comparison with conductors, is the additional energy required to excite a population of SE's across the insulator bandgap [2,3,9]. This suggests the average energy, ε, required to excite an SE inside an insulator must be close to the insulator bandgap, $\varepsilon \sim E_g$. Based on the assumption that ε is equal to the electron-hole-pair creation energy, Alig and Bloom [9] have used energy and momentum conservation arguments, along with empirical data for a wide range of insulators, to offer an average SE creation energy as $\varepsilon \sim 2.8 \cdot E_{gap}$, where the factor of 2.8 results from momentum and energy conservation arguments. This means that $\sim E_o/(2.8 \cdot E_{gap})$ electron/hole pairs are created by each PE, down to the depth $R(E)$. As indicated above, this treatment for SE production in insulators only applies to materials that have not been charged. As described in more detail in Thomson [3] and Meyza *et al.* [14], the ranges of incident electrons in charged insulators can be significantly altered by internal charge distributions and resulting high internal electric fields.

2) *Secondary Electron Transport:* In general, the mean SE escape depths for insulators are greater than for conductors and semiconductors [15]. For conductors, the probability for electron-electron and electron-plasmon scattering in the conduction band is greater than it is for insulators due to the greater number of free charge carriers. For semiconductors, although there are fewer charge carriers in the conduction band, the probability for valence electron scattering is greater due to the relatively small energy bandgap [2,11,15]. The insulator bandgap (for insulators, typically 5 eV $< E_{gap} <$ 10 eV), which is typically larger than the mode energy of the emitted electrons (typically 2eV to 5 eV; see Figures 1b and 4b) inhibits electron-electron scattering for SE near the conduction band minimum, thereby increasing λ_{SE}. For SE with $E \leq E_{gap}$, the dielectric material is then largely transparent. Phonons and electron-hole pair recombination dominate transport of SE [3,17]. During their transport in the conduction band, some electrons of the generated electron/hole pairs may be trapped on localized defect sites in the forbidden region of the band gap.

3) *Emission:* The electron affinity is typically used as the relevant surface barrier for insulators. Details of the relation of band gap and electron affinity to the escape probability are discussed elsewhere [2,3,9].

Thomson provides a more complete review of topics related to the three stage models [Clint dis].

Accumulated charge in insulators or surface charge for biased conductors interact with incident and emitted charged particles through Coulomb interactions which affects all three stages of the electron emission models. Ideal, one needs to develop an equation that gives the SE yield in terms of accumulated charge or fluence of the form

$$\delta(E_O, Q) = \int_0^{R(E_O, Q)} n(x, Q; E_o) \cdot f(x, Q; E) \cdot B(E, Q) \, dx \qquad (6)$$

based on physical principles. Thomson [3] and Sim [5] provide discussions of such a development. However, to date there is no quantitative theory for yields of charged materials based on the three stage models. The experimental evidence presented in this paper does provide some insight for the development of such a model.

Models of Electron Emission Spectra

An alternative approach for studying the escape of SE electrons from a material's surface potential barriers is provided by the Chung and Everhart [8] model of electron emission spectra, which expresses the energy distribution of emitted SE in terms of the work function for metals (or electron affinity for insulators). The model starts with a

population of SE's that have been excited by incident electrons (or photons or ions), and uses the exponential transport and escape probability expression given by Eq. 4 to determine whether an SE created at some depth within the solid will reach the surface. The model also considers surface energy barriers (i.e., work function or electron affinity). The predicted energy distribution of emitted SE's is given as:

$$\frac{dN(E;E_o)}{dE} = \frac{k}{E_o}\frac{E}{(E+\phi)^4} \tag{7}$$

where $N(E)$ is the number of emitted electrons, E is the SE emission energy, k is a material-dependent proportionality constant, E_0 is the incident beam energy, and ϕ is the material surface barrier. The SE yield in terms of $N(E)$ is given by

$$\delta(E_O) = \int\limits_{0\,eV}^{50\,eV} \frac{dN(E;E_o)}{dE}\,dE \tag{8}$$

A more thorough explanation of the Chung and Everhart model is provided in Davies [32]. Measured emission spectra are presented later and shown in Figures 4 and 5.

The polarity and magnitude of insulator charging is dependent on the incident electron energy, as discussed above. The response of low energy emitted electrons to surface biasing is illustrated in Figure 3a. For negative charging conditions, with E_o above E_2 or below E_1, the steady-state condition is dependent on raising the negative surface potential such that either the SE distribution is pushed above 50 eV (fast negative charging mechanism), or the landing energy of incident beam is decreased to a value close to E_2 (slow negative charging mechanism). For the fast negative charging mechanism, negative charging increases the insulator surface potential barrier by an amount $-e|V_s|$. SE near the (arbitrary) 50 eV division have increased kinetic energy that means they are registered as BSE. Hence, the resulting SE electron yield emitted from a negatively charged samples can be expressed as an integral of the uncharged spectrum (taken at the same incident energy) with the integration limits extending from zero up to the 50 eV division plus the negative surface potential [10,11]. This is illustrated in Figure 3b, where the higher-energy portion of the SE spectrum (represented by the shaded area in the figure) is transferred to the BSE yield. Consequently, only the unshaded area of the electron energy spectrum contributes to the charged SE yield.

$$\delta(E_O,Q) = \int\limits_{0\,eV}^{50\,eV-e|V_s(Q)|} \frac{dN(E;E_o)}{dE}\,dE \tag{9}$$

Note there is a commensurate increase in the BSE yield and hence no net change in the total yield for the fast negative charging mechanism. For ideal insulators, Reimer [11] has expressed the negative surface potential resulting from the slow charging mechanism in terms of the incident electron landing energy, E_L, and the incident beam energy, E_0. This expression has been termed the total yield equation:

$$E_L(Q) = E_o - e|V_s(Q)|, \tag{10}$$

where e is the fundamental electron charge, and V_s is the negative surface potential. For insulators with large, but finite, resistivity, an additional time-dependant term must be added to account for accumulated charge that is dissipated as a leakage current through the thin-film insulators [3]. Sim provides a more complete discussion of this process [5].

Between the total-yield crossover energies, E_1 and E_2, the magnitude of insulator charging is positive (since the total yield is greater than one), and the insulator attains a steady-state surface potential of just a few volts [10,11]. This positive charging increases the insulator surface potential barrier by an amount eV_s, where V_s is the positive surface potential. Hence, the resulting total electron yield emitted from a positively charged specimen can be expressed as an integral of the uncharged spectrum (taken at the same incident energy) with the integration limits extending from the positive surface potential up to the incident beam energy [10,11].

$$\delta(E_O,Q) = \int\limits_{eV_s(Q)}^{50\,eV} \frac{dN(E;E_o)}{dE}\,dE \tag{11}$$

This is illustrated in Figure 3c, where it is shown that positive surface charging prohibits the escape of lower-energy SE's, thus suppressing the lower-energy portion of the SE spectrum (represented by the shaded area in the figure). Consequently, only the unshaded area of the electron energy spectrum (above eV_s) contributes to the charged electron yield. As explained by Thomson [3], this provides a method for calculating an insulator's positive surface potential by measuring the steady-state (charged) electron yield along with an accompanying electron spectrum at the same incident energy. It follows that the fraction of the SE yield returned to the surface is

$$\frac{\delta_i(E_o, Q_i)}{\delta_o(E_o)} = \frac{\displaystyle\int_{eV_s(Q_i)}^{50\,eV} \frac{dN(E;E_o)}{dE}\, dE}{\displaystyle\int_{0\,eV}^{50\,eV} \frac{dN(E;E_o)}{dE}\, dE} \tag{12}$$

as shown in Figure 3d. This assumes that the distribution of emitted electrons given by Eq. 7 does not change shape or amplitude with charge accumulation, but only shifts peak position as discussed above. Experimental evidence for both biased conductors and charged insulators suggests this is reasonable assumption [5,10]. Between the crossover energies, typical fractional SE yields for insulators approach values of 0.2-0.6, corresponding to positive surface potentials of 4-10 V. Therefore, no change in BSE yield is expected.

A simple model of the total yield as a function of charge follows. The modified total yield for accumulated charge Q for an incident energy E_o is

$$\sigma(E_o, Q) = \eta(E_o, Q) + \delta(E_o, Q) = \eta(E_o) + \delta(E_o) \cdot \left[\frac{\delta(E_o) - \delta_{return}(E_o, Q)}{\delta(E_o)} \right] \tag{13}$$

with the magnitude of the returned SE given by $\delta_{return}(E_o, Q)$, the SE yield of an uncharged insulator is given by $\delta(E_o)$, and the fraction of the SE electrons that escape is given by the term in square brackets. Substituting Eq. 12 into Eq. 13,

$$\sigma_i(E_o, Q_i) = \eta(E_o) + \delta(E_o) \left[\frac{\displaystyle\int_{eV_s(Q_i)}^{50\,eV} \frac{dN(E;E_o)}{dE}\, dE}{\displaystyle\int_{0\,eV}^{50\,eV} \frac{dN(E;E_o)}{dE}\, dE} \right] \tag{14}$$

The surface potential as a function of incident charge can be approximated using Eq. 16, developed below. A more advanced version of this model accounts for the fact that yields are modified as the landing energy, $E_L(Q)$, is modified with charge accumulation; thus $\delta(E_o) \rightarrow \delta(E_L(Q))$ and $\eta(E_o) \rightarrow \eta(E_L(Q))$ in Eq. 14 and $\sigma \rightarrow \sigma(E_L(Q))$ in Eq. 16 for $V_s(Q_i)$. Note an expression similar to Eq. 14 can also be developed for the slow negative charging mechanism using Eq. 9. Thomson provides a much more detailed treatment for the development of Eq. 14, including analytic expressions based on solutions to Eq. 7 [3].

Models of Electron Yield Decay Curves

Yet another approach for studying the effects of accumulated charge on electron emission is the phenomenological model of electron yield decay curves as a function of accumulated charge or fluence [3-5,15]. Let the uncharged yield be σ_0 and recall that the yield approaches unity as large charges accumulate. A reasonable phenomenological model for an equation that gives decay curves in terms of accumulated charge is then

$$\sigma_i = 1 + [\sigma_o - 1] \cdot \exp\left[-\alpha(Q, E_o) \cdot \left(\sum_{j=1}^{i} Q_{(j-1)} \right) \right] \tag{15}$$

where σ_i is the yield after the ith pulse and Q_j is the charge deposited in the jth pulse. The exponent α has units of inverse Coulombs, and is a decay constant related to the charging time constant of the sample and system, representing the rate at which the sample exponentially approaches a (quasi-) steady state with successive incident charge pulses. Alpha provides first step in modeling dependencies of the material properties on charge and may itself be dependant on both incident energy and accumulated charge, $\alpha = \alpha(Q, E_o)$.

As shown in simulation [14]and experiment (see below,[3]), the decay constant, α, is energy dependent. One would expect it to be relatively large for energies $E_1 < E_0 < E_2$, since positive surface potentials need to rise only to a few volts to trap the majority of escaping SE's, thus achieving a steady-state condition very quickly. However, above E_2, the steady-state condition is dependent on raising the negative surface potential such that either the SE distribution is pushed above 50 eV (fast negative charging mechanism), or the landing energy of incident beam is decreased to a value close to E_2 (slow negative charging mechanism). For $E_0 > E_2$, since the total electron yield is lower, and surface potentials must reach several hundred to thousands of volts to reach steady state, one would expect the time constant to be much smaller.

Models of Distributions of Accumulated Charge and Surface Potentials in Insulators

As discussed above, the polarity and magnitude of the charging depends on the incident electron energy. For biased conducting materials, the charge resides near the surface based on Gauss' Law. For ideal insulators, one assumes that SE do not move appreciable distances within the material and that the charge distribution is the same as the production profile. The simplest model of charge distribution in an insulator is that all charge is deposited in a simple thin layer at a depth equal to $\lambda_{PE}(E_o)$. This follows from the Bethe approximation for SE production used in the Sternglass formulation of the yield formula [18]. The constant loss model for the yield formula [7,19] assumes that SE are produced by the PE uniformly in the material up to the range, $R(E_o)$, leading to a uniform negative charge distribution with an incident energy dependant depth. Various other power law formulation for the yield curve lead to similar negative charge distribution with an incident energy dependant depth. Most notable is the Young model with a power law exponent of $n=1.35$, as opposed to 1 for the constant loss model [19].

Finite resistivity allows redistribution of charge within the insulator, leading to more complicated internal charge distributions [20]. Previous models of insulators have shown the internal charge distributions (both evolving distributions, as well as static charge distributions), resulting from incident electron irradiation, form multiple alternating positive and negative charge layers [6,14,21-24]. Measurements of internal charge distributions of thin-film insulators confirm the general nature of these distributions [25-27], including a number of papers in these proceedings [28-30]. Thomson provides a useful review of the literature on charge distributions within insulators, with application to electron emission from insulators [3]. Net positive (negative) charge will build up when the total number of electrons leaving the insulator sample is greater than (less than) the total number of incoming electrons. However, the spatial and charge-polarity configurations of these layers can be complex and difficult to predict; the distributions can depend on a number of factors that includes the magnitude of electron yield, electron yield crossover energies (particularly E_2), material resistivity (both innate and radiation-induced conductivity), dielectric strength, electron trapping and detrapping rates, incident electron penetration depths, mean SE escape depths, and incident electron fluxes and energies. Three charging scenarios for different incident energy regimes are presented:

(i)   If the incident electron energy is below E_1, (<100 V for most good insulators) net negative charging results, since few SE's are excited by absorbed electrons. The distributions typically are not too complex.

(ii) For incident electrons with $E_1 < E_o < E_2$, more electrons will be emitted from the insulator than are incident, and net positive charging will occur. Incident electron penetration is only somewhat larger than the SE escape depth, resulting in a small deep negative charge region and a larger positive charge region closer to the surface (see Figure 2b). The electric field from the negative charge again retards further incident electron penetration and acts to drive more low energy SE's from the sample, thereby enhancing the positive charge region [5,11]. The electric field from the positive charge region in turn acts to re-attract the lowest energy SE emitted from the surface (gray region in Figure 3c), thereby establishing a shallow negative surface charge region. A double charge distribution (positive-negative) is formed where the positively charged region, from SE depletion, occurs between the surface and λ_{SE}, and a negatively charged region, from embedded incident electrons, occurs between the surface and R. For this charging scenario, the simple Dynamic Double Layer Model (DDLM) has been presented in the literature [21,22,31] to predict ensuing internal electric fields and potentials. Figures 2b and 2c show the internal charge distribution and electric field for such a DDLM.

(iii) The internal charge distribution for an energy above E_2 (>1 keV for most insulators), has a large, deeply embedded negative charge as a result of the large penetration depth of the higher energy incident electrons (up to several microns), exciting SE's (escape length tens of nanometers) that are too deep to escape from the material. As the negative charge builds up, the resulting electric field reduces the energy of additional incident electrons and inhibits

their range. In addition, there is a depletion region of small positive net charge near the surface where low energy SE's can escape the surface assisted by the electric field from the large negative charge distribution.

For charge distributions such as the DDLM deposited over a thickness d, the surface potential can be approximated assuming a parallel-plate capacitor geometry with a total incident charge of Q_o [3,22]:

$$Vs = \frac{Q_o(\sigma - 1)d}{\varepsilon_o \, \varepsilon_r \, A_o} - \frac{\sigma \, Q_o \, \lambda_{SE} + Q_o \, R}{2 \, \varepsilon_o \, \varepsilon_r \, A_o} \quad \xrightarrow[d >> R, \lambda_{SE}]{} \quad \frac{Q_o(\sigma - 1)d}{\varepsilon_o \, \varepsilon_r \, A_o} \cdot \qquad (16)$$

The thin-film capacitor geometry is a reasonable approximation since charge deposition area, A_o, given by the electron beam radius, R_{beam}, is much greater than d, R and λ_{SE} (for studies reported here, R_{beam} was on the order of 0.5 mm, whereas insulator thicknesses ranged from 1-50 μm). Furthermore, it can be seen that the first term in Eq.16 dominates if the insulator thickness, d, is much greater than R or λ_{SE} (R generally did not exceed ~1 μm for the incident energies reported here); this approximation is equivalent to assuming a uniform charge distribution. Equation 16 is equally as valid for approximating the change in surface potential of both net positively ($\sigma > 1$) and net negatively charged insulators ($\sigma < 1$), since as σ decreases below unity, the surface potentials becomes negative.

Experimental Methods

Instrumentation and Methods

We briefly describe the instrumentation used at Utah State University (USU) to study electron emission from insulators. Three vacuum chambers available at USU are equipped with electron, ion, and photon sources and detectors, and have extensive surface analysis and space environment simulation capabilities [1]. Electron emission measurements are performed in a ultra-high vacuum chamber (base pressure < 10^{-8} Torr) to minimize surface contamination that can substantially affect emission properties [32,33]. Electron sources provide electron energy ranges from ~50 eV to ~30 keV and incident electron currents (1-100 nA) with pulsing capabilities ranging from 10 ns to continuous emission [1-3]. A hemispherical detector features an aperture for incident electron/ion admission and a fully-encasing hemispherical collector for full capture of emitted electrons with a retarding-field analyzer grid system for emitted-electron energy discrimination [2,3,5]. A sample stage holds 11 samples that can be positioned in front of various sources and detectors and is detachable for rapid sample exchange.

A DC method with a continuous, low-current beam of electrons is used to measure electron emission from conducting samples. Charge added to or removed from a conductor via electron emission can be easily and rapidly replaced by connecting the sample to ground [1,2]. Reviews of methods used by previous investigators to study insulator emission are found in Thomson [3] and Reference 35 [35]. The system at USU to measure electron emission from insulators uses a combination of methods to control the deposition and neutralization of charge [3,5,34,35]. Charge deposition is minimized by using a low current beam (~10-30 nA) focused on a sample area of ~1 mm^2 that is delivered in short pulses of ~5 μsec. Each pulse contains ~10^6 electrons/mm^2. This amount of charge is estimated using Eq. 16 to change the surface potential by only 10-100 mV/pulse (positive) and requires ~10^4 pulses to achieve an ~1 nA/cm^2 dosage that typically causes discharge in space. The pulsed system uses custom detection electronics with fast (1-2 μs rise time) sensitive/low noise (10^7 V/A / 100 pA noise level) ammeters [Clint dis, SCC8 insulator inst]. Charge dissipation techniques include a low energy (~1-10 eV) electron flood gun for direct neutralization of positively charged surfaces and a variety of visible and UV light source for neutralization of negatively charged surfaces through the photoelectric effect [3,5]. Sample heating to ~50-100 °C has also been used for dissipation of buried charge by thermally increasing the sample conductivity.

To measure points on the yield curves at a particular energy, a series of ~10 to 50 pulses at constant incident energy are measured with ~5-10 sec of neutralization between each pulse using both low energy electron flooding and visable-ultraviolet flooding (see Figure 7 below). Similar series of pulses at a fixed incident energy, taken without neutralization, constitute so-called decay curves.

Sample Descriptions

Measurements on three common spacecraft insulators are reported here; additional measurements on these samples are found elsewhere [3-5,34,36]. The Kapton™-aluminum samples were composite materials sold by Sheldahl Technical Materials for applications as a low emissivity thermal control coating material for spacecraft. The 8 μm thick 10 mm diameter polyimide Kapton H™ substrate was vapor coated with a ~0.1 μm Al backing. The 25 μm thick 10 mm diameter polyimide Kapton H™ substrate was vapor coated with a ~0.1 μm Au backing. The chromic acid anodized Al alloy (Al2219) sample (2 mm thick, 10 mm diameter with a 1.3 μm chromic acid anodized surface coating on each side)

was provided by the NASA Marshall Space Flight Center. This material is used throughout the International Space Station body as a structural material and for micrometeriod and orbital debris shielding [36]. These insulator samples were cleaned using acetone and methanol before introduction into a vacuum chamber operating at 10^{-7} Pa, but were not ion sputtered.

Thin-film copper samples are coated with NuSil CV-1147, a controlled volatility RTV silicone coatings used to bond solar cells to Kapton™ sheeting on the International Space Station. The RTV material was relatively volatile; concerns that this material would produce contamination layers on ISS surfaces prompted the investigation of these thin-film materials on a conducting substrate [37]. Similar contamination layers have been shown to potentially have a large impact on the charging of spacecraft surfaces [45]. The thin-film sample was prepared by McDonald Douglass of Boeing Corporation, where the 34±3 μm coating was sprayed onto one side of a 10 mm dia. copper substrate, and were vacuum baked at 65 °C for 1 hr at ~10^{-3} Torr. The bake out procedure was designed in part to mimic conditions the materials would experience in the space environment and also reduced possible outgassing of volatile components in the USU vacuum chamber during electron emission measurements [37]. No cleaning methods at USU were used before introduction to vacuum.
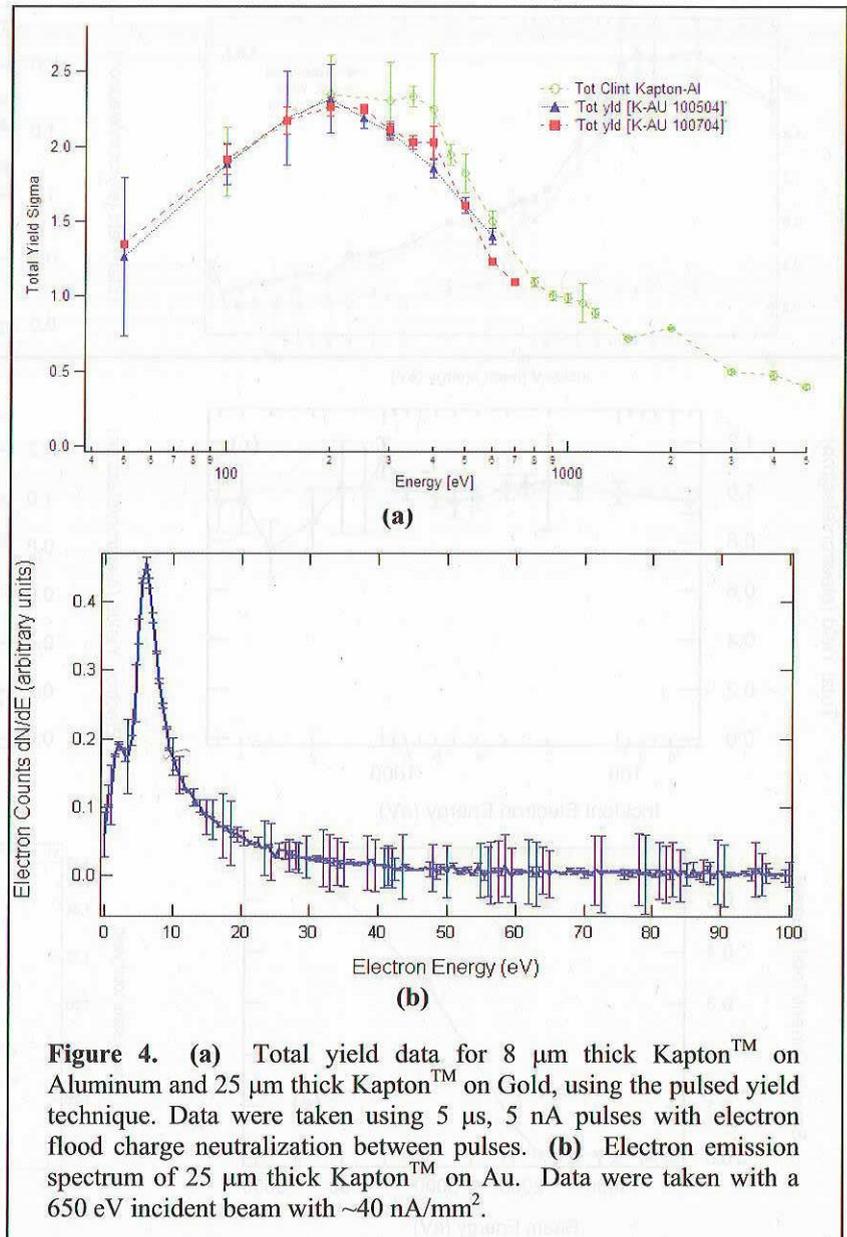
Measurements are also presented for a high purity (6N) polycrystalline

Figure 4. (a) Total yield data for 8 μm thick Kapton™ on Aluminum and 25 μm thick Kapton™ on Gold, using the pulsed yield technique. Data were taken using 5 μs, 5 nA pulses with electron flood charge neutralization between pulses. (b) Electron emission spectrum of 25 μm thick Kapton™ on Au. Data were taken with a 650 eV incident beam with ~40 nA/mm².

Au sample from ESPI Metals. The sample was Ar ion sputtered *in situ* and the surface cleanliness was verified with Auger Electron Spectroscopy to have only minimal carbon contamination at the atomic monolayer level [38].

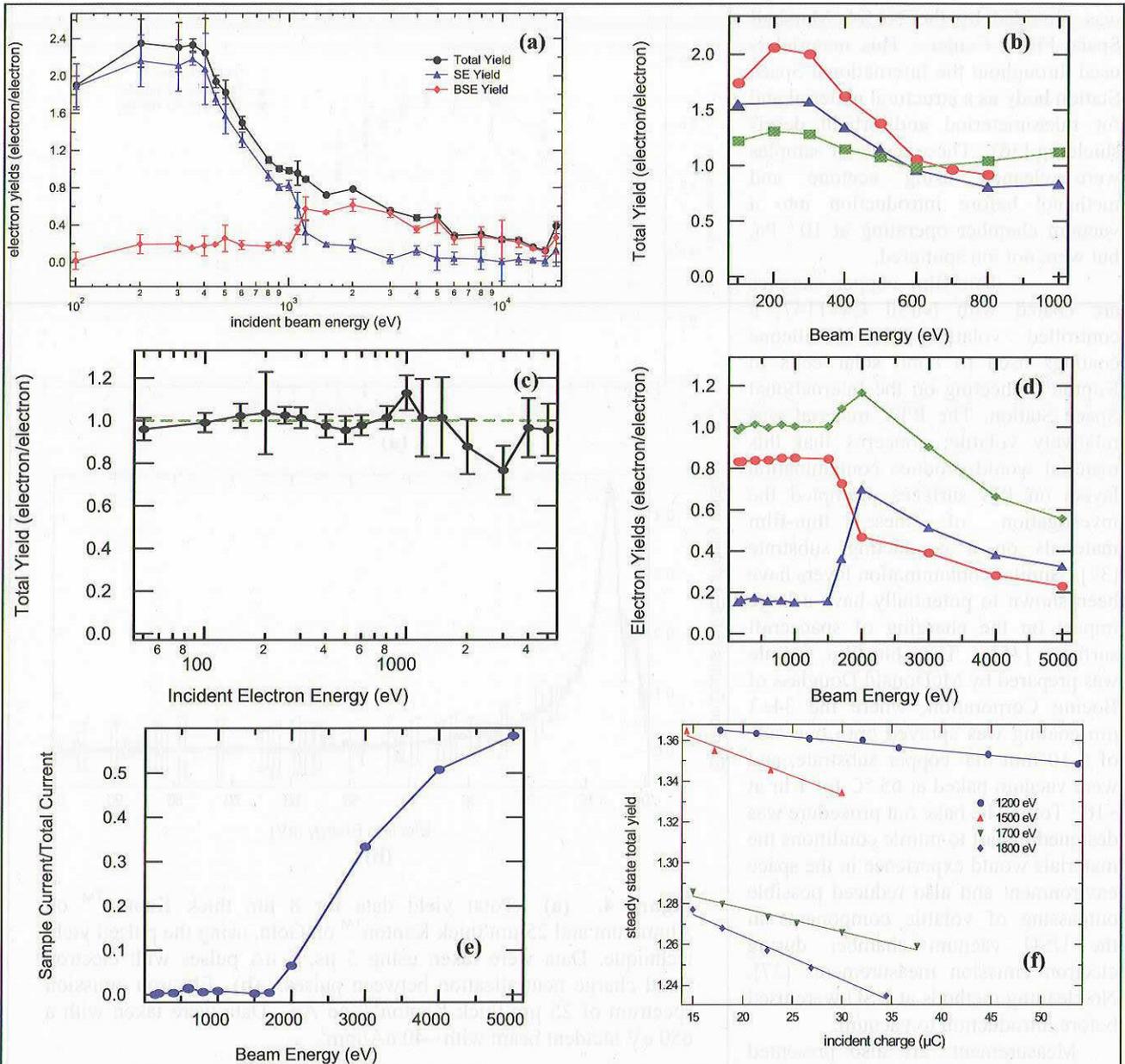## Effects of Charge Accumulation on Electron Emission

We now present experimental results to explore the effects of charge on various emission measurements of insulators. First, measurements of reliable yield curves for uncharged insulators are shown. Evolution of total, backscattered and secondary yield results over a broad range of incident energies in response to accumulated charge are presented. Next, we present measurements of various changes to the electron emission spectra that result from charge accumulation. Finally, decay curves are presented that show the evolution of the electron yield for specific incident electron energies as a function of incident electron fluence.

Yield Curves and Emission Spectra of Uncharged Insulators

Pulsed yield methods with alternating charge neutralization used at USU have been shown to produce reliable and reproducible measurements of the absolute total yield curves of insulators [1,3]. Typical accuracies for absolute yields are 5-10% for insulators and a few percent for conductors; measurement precision is significantly less. Figure 4a shows three total yield curves measured for 8 μm thick Kapton™ on Aluminum and 25 μm thick Kapton™, on Au

Figure 5. *Effects of Charge Accumulation on Insulator Yields* (a) *Yield Curve with Fast Negative Charging Mechanism above E₂*—Combined pulsed total, SE, and BSE yield curves for Kapton™-aluminum. BSE yields increased and SE yields decreased past E_2, due to the additional energy given to escaping SE's by increasing negative surface potentials. (b) *Yield Curve in Transition*—Pulsed total yield of 1.3 μm anodized layer on an Al 2219 alloy sample tends toward unity as sample charges. Even small charge accumulation was found to have substantial effect on yield curves. Three consecutive first (●), second (▲), and third (■) pulsed-total yield curves (5 μs, 40-60 nA impulses) were taken without use of any neutralization techniques. (c) *Yield Curve in Steady-state Charge Equilibrium*—Pulsed total yield curve of RTV-silicone was taken without use of any neutralization techniques. Yields fluctuate around unity for all incident energies measured. (d) *Yield Curve Showing Sample Breakdown*—Total (♦), SE (●), and BSE (▲) yields curves for 1.3 μm anodized Al sample measured under DC bombardment that charges the sample to equilibrium. Negative surface charging is observed above ~1500 eV as E_2 is exceeded, leading to increased BSE and decreased SE yields. At ~2000 eV the total, SE and BSE yields all begin to decrease, indicative of sample breakdown. (e) Monitoring sample current for the data set in (d) confirmed dielectric breakdown at ~2000 eV, where the sample began to conduct DC current. (f) *Yield Curves with Slow Negative Charging*—Dependence of evolving (quasi-)steady state total yields with incident energy and electron fluence. For $E_o<E_2$, the initial yield and slopes show no clear trends with energy (not shown; see [3]). For $E_o>E_2$, the initial yields values are seen to depend on energy, and the measured slopes were consistently negative.

using the pulsed yield technique. Data were taken using 5 μs, 5 nA pulses with electron flood charge neutralization between pulses. Note the level of agreement (at most ±10%) between the curves for three separate Kapton samples taken ~1 year apart by different researchers. These measurements showed very little evidence of surface charge accumulation. Based on these data we estimate for Kapton that E_I~(30±10) eV, E_2~(962±25) eV, σ_{max}~2.4±0.1 at E_{max}~(195±10) eV and n=1.68 (which is related to the rate at which the yield approaches the asymptotic limit, $\sigma(E_o \rightarrow \infty) \rightarrow 0$) [3].

　　　　Figure 4b shows an electron emission spectrum of unneutralized 25 μm thick Kapton™ on Au. Data were taken with a 650 eV continuous incident beam with ~40 nA/mm². This beam energy is somewhat less than the estimate dvalue of E_2~(962±25) eV [3], with a measured uncharged yield of ~1.25 (see Figure 4a). Therefore, the sample is expected to be at a small positive equilibrium potential, with only modest charging. The peak in the emission spectra from Kapton is at ~6 eV; this suggests there may be a small negative sample charge. The small peak visible at ~2 eV is from secondary electrons produced by the sample BSE scattering off of the inner grid [5].

Yield Curves of Charged Insulators

　　　　Figure 5a shows a yield curve with no significant charging effects below E_2 and only the fast negative charging mechanism above E_2. The figure shows a composite of total, secondary and backscattered yield curves for an 8 μm thick Kapton sample on Al [3]. Ten pulses, each 5 μs at ~35 nA, were averaged for each yield data point, and the electron flood gun was triggered between each incident pulse to neutralize any positive surface charging. However, for $E_0 > E_2$, although the electron flood gun was still employed between each incident pulse, the gun was not expected to neutralize negative surface charging. As can be seen by comparison of Figures 4a and 5a, for $E_0 < E_2$, the total electron yields did not appear to be strongly altered by repeated electron pulsing, since, within the data error, the total yields decreased smoothly with increasing incident energy (as they should for $E_0 > E_2$). However, from the data for $E_0 > E_2$, it was observed the SE and BSE yields were significantly altered with repeated pulsing. Specifically, once E_2 was traversed (between 950-1000 eV), the BSE yields jumped in magnitude by a factor of three to values that approached total yields, and the SE yields approached zero. This jump was attributed to the fast negative charging mechanism described above (reference Figure 3b), where upon crossing E_2, the insulator surface potential charged negatively beyond 50 V, accelerating escaping SE's to energies >50 eV. Consequently, the major fraction of the total electron yield was comprised of electrons with energies >50 eV, which were therefore registered as BSE's by our detector. Hence, for $E_0 > E_2$, although the total electron yields remained accurate, the designation as SE and BSE yields were not.

　　　　Figure 5b shows yield curves in transition from the uncharged yield curves to yield curves at equilibrium charge with yield approaching unity. As discussed above in association with Figure 3, the electron yield of insulators tends to unity as charge is accumulated. Even small charge accumulation was found to have substantial effect on yield curves. Three consecutive pulsed-total yield curves (5 μs, 40-60 nA/mm² impulses) were taken without use of any neutralization techniques [3,4]. After just a few incident pulses, the subsequent yield curves were significantly dampened towards unity, even though the incident source was only depositing ~10⁶ electrons/pulse over a beam-spot area of ~10⁰ mm². Treating the sample as a standard parallel plate capacitor (with an area of the beam spot), this amount of charge was estimated to change the surface potential by only 10-100 mV/pulse (positive). However, a significant portion of SE's are emitted with energies less than 5 eV (see Figure 3c) such that a cumulative positive surface potential of <1 V can significantly suppress escaping SE's.

　　　　Figure 5c shows a yield curves that has reached charged steady-state with yields at all incident energies, approximately equal to unity. The total yield curve is for a CV-1147 RTV-silicone sample [3,4]. Each yield point was the average of 10 pulsed-yield measurements (5 μs pulses with amplitude ~30 nA) and no neutralization was used after each pulse such that total yields quickly approached equilibrium. The yield is observed to fluctuate around unity over a wide range of incident energies and does not exhibit any evidence of the peak observed in uncharged yield curves.

　　　　Figures 5d and 5e illustrate a case in the extreme, where very large negative charge build up and leads to dielectric breakdown. DC-yields were taken first using a continuous electron source at ~20 nA beam current for an Al2219 alloy sample (2 mm thick, 10 mm diameter with a 1.3 μm chromic acid anodized surface coating on each side) [3,4]. As shown in Figure 5d, for energies ranging from 100 eV to 1500 eV, the insulator quickly charged such that a steady-state current equilibrium was established where the total yield reached unity, and no net current flowed to or from the sample. Negative surface charging is observed above ~1500 eV as E_2 was exceeded, leading to increased BSE and decreased SE yields (the same fast negative charging mechanism observed in Figure 6a). At ~2000 eV the total, SE and BSE yields all begin to decrease, indicative of sample breakdown. Monitoring Al2219 sample current (see Figure 6d) confirmed that no current flowed until ~2000 eV, where the sample began to conduct DC current following dielectric breakdown of the anodized coating. For this measurement, the exact value of the surface potential at electrical breakdown was not measured, but from the known thickness and dielectric strength for Al₂O₃ (see Ref. 3) it was estimated to be ~45 V, with an electric field strength of ~3·10⁷ V/m. Previous measurements on this material have demonstrated a breakdown potential ranging from 60-80 V [36]. Frederickson has estimated that the electric field at breakdown occurs at ~10⁷ V/m for most dielectric materials [39,40].

Figure 5f shows the effect of larger charge accumulation on yields termed the slow negative charging mode above; the effects are attributed to material modification due to charge accumulation and energy deposition. A monochromatic continuous electron beam was used to deposit large amounts of charge in an 8 μm thick Kapton on Al sample, and the evolution of the steady state total yields of were monitored as a function of total incident electron fluence and energy [3]. The incident current varied between 20-30 nA (depending on the energy). The sample was irradiated up to $2 \cdot 10^3$ s for each energy (cumulative incident charge densities ranged from 10-60 μC/mm^2), and total yields were plotted versus cumulative incident electron charge ($I_0 \cdot$time). For $E_0 < E_2$, their existed no clear dependence between the total yields, which remained near unity, and incident charge (not shown here; see [3]). However, for $E_0 > E_2$, total yields consistently decreased (slowly) with incident electron charge. The rate of decrease was only 1-4 percent over 30-60 μC of incident charge, but the trend was very consistent for each steady state yield set taken beyond E_2. It did not appear from the data that the slope magnitudes depended on incident energy, but the initial magnitudes of the steady state yields did. These data were consistent with predictions from Cazaux [17] and Reimer [11] that steady state yields should decrease with continued incident electron irradiation due to radiation induced conductivity as well as the additional defects and electron trapping that are created by the incident beam and high internal electric fields due to internal charge build up. Furthermore, Liehr *et al.* [41] reported similar decreases in electron yield parameters with continued electron irradiation on polyethylene, finding a decrease in E_2 by 26% after irradiating with 20 mC of incident charge.

Emission Spectra of Charged Insulators

Figure 6a shows the emission spectra of a negatively biased conducting gold sample measured using a 1 keV incident beam. The sample was irradiated with a continuous electron beam, and energy distributions of the emitted electrons were taken. Measuring shifts in the SE spectral emission peak provides a method for accurately determining the sample surface potential while under continuous electron bombardment [5]. Due to the repulsion of emitted SE's from the negatively biased sample, the emission peak is right-shifted to values corresponding to the sample potential. The bias potentials were -2, -5, -10 and -15 V, respectively, from left to right. The sample potential can be accurately determined by the position of the Au emission peak measured with respect to the fixed peak at ~1.8±0.5 eV. A fixed "false" SE emission peak observed in all the spectra is caused by electron scattering from a grounded inner detector grid of our hemispherical grid retarding field analyzer positioned between the sample and the retarding grid [5,6]. This false SE peak did not vary with sample type or bias, and was taken as a ground-reference potential for shifted sample SE peaks. The sample bias determined by the Au peak position agrees with the corresponding applied bias to within ±0.5 eV. The decrease in amplitude of the biased emission spectra result from the decrease in yield as the landing energy is reduced by the bias potential. Sim presents a more complete study of both positive and negative sample bias and the effects of ungrounded grid potentials and varying incident energy; the results confirm our description of the shifts in peak position and amplitude changes as a function of conductor bias [5]

Similar spectral measurements made for an insulating RTV sample near the second crossover energy, are shown in Figure 6b [3,34]. Between 1200 eV and 1250 eV (and for lower incident energies not shown) the spectral amplitude and peak position remained unchanged, indicating no surface charging. At incident energies of 1300 eV and higher, the spectral peak shifts to right as the RTV sample charges negatively. From these measurements, we conclude that $E_2 \sim 1275$ eV for the RTV sample, consistent with other measurements made using different methods [3]. The fact that the observed peak shifts were less than the increased beam energy suggests that the RTV sample had a modest resistivity so that significant (but not complete) leakage occurred in the time between spectral measurements (refer to Eq. 16) [3]. Measurements of the resistivity of the RTV sample using a modified ASTM-257 constant voltage method [42] found $\rho \sim 10^{15}$ Ω-cm, which corresponds to a charge decay time of ~5 min [37,43], consistent with this hypothesis.

Similar spectral measurements were made for the anodized Al sample [1,3]. The incident beam energy was increased for each successive spectral measurement (starting from 200 eV up to 1300 eV) until signs of breakdown occurred. The right-shifting of the SE emission peak was used to determine the magnitude of the sample potential. From the data (see Figure 6, [1]), it was observed that the sample potential remained negative at energies between E_1 and E_2, and increased in magnitude with increasing incident energy. A negative potential is not normally expected between the crossover energies since the total electron yield for nearly all materials is greater than unity in this energy regime (and positive surface charging should occur). However, previous experimental studies on Al_2O_3 have shown that the measured polarity of charging does not always correspond to that predicted by the electron yield parameters [17,21]. A possible explanation for such behavior for our specific sample is that the previous electron irradiation produced residual trapped charge (embedded in the bulk) that provided a cumulative negative sample potential regardless of any positive SE surface charging taking place at beam energies between the crossovers. The amplitude of the emission spectra decreased markedly between 1000 eV and 1250 eV, indicative of modifications in the total yield as the second crossover was traversed. This range of second crossover energy is reasonably consistent with that determined from data in Figure 5d above. As shown in Figure 6c, as the beam energy was increased to 1250 eV and 1300 eV the surface potential reached -21±2 V and -31±2 V, respectively. Electrical breakdown was observed to occur at ~2000 eV (see
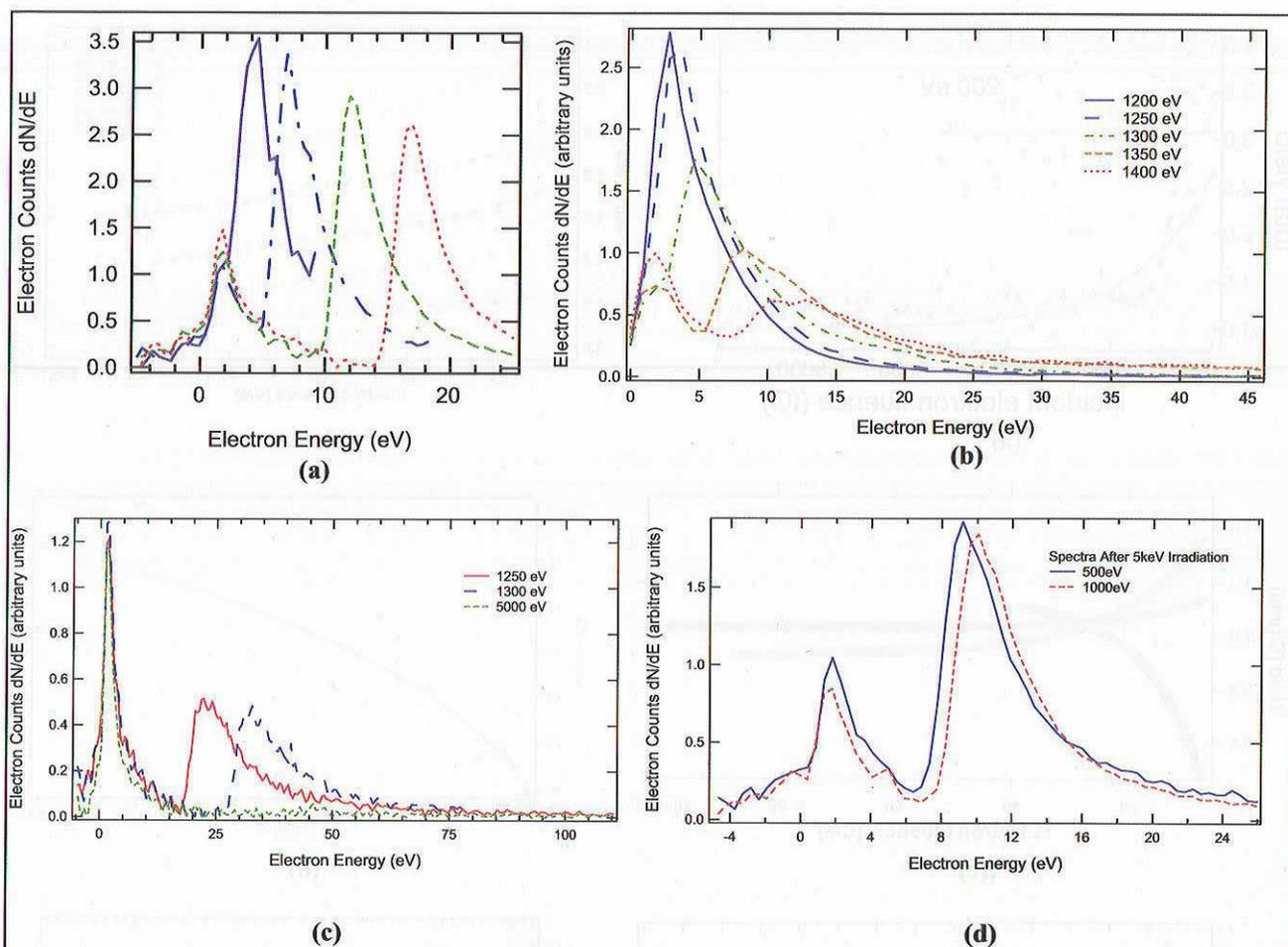
Figure 6. Modification of electron emission spectra by charge accumulation. **(a)** SE spectra of a negatively biased conductive Au sample with the inner grid grounded. The bias potentials were -2, -5, -10 and -15 V, respectively from left to right. **(b)** The onset of negative sample charging is evidenced by the decrease in spectral intensity for an RV sample, beginning at incident energies above ~1250 eV. **(c)** The drop to near zero amplitude in the emission spectra of anodized Al at an incident energy above 1300 eV indicates a breakdown. **(d)**. Observation of hysteresis in the electron emission spectra. After prolonged exposure to higher energy (5 keV) fluxes, spectra from an anodized Al sample shift to lower shifts in the sample peak positions and show that V_s remains locked at 8 eV.

Figures 5d and 5e). This is consistent with the emission spectra taken at 5000 eV where the amplitude has drop to nearly zero.

Once breakdown had occurred, the anodized aluminum sample was irradiated for 10^3 s at 5 keV beam energy to determine if subsequent emission spectra would be affected by increased charge stored deep within the material. Subsequently, the incident beam was once again lowered and emission spectra were measured [1,3]. The sample potentials measured at both at 500 eV and 1000 eV no longer showed dependence on incident beam energy, but remained locked at -8±1 V. This was in contrast to measurements before the intense high energy irradiation that found shifts of 11±1 V for 500 eV and 17±1 V for 1000 eV. This demonstrated hysteresis in the sample emission, where residual charge from the high-energy incident beam caused a breakdown which increased sample radiation-induced conductivity and did not permit subsequent large charging to be sustained.

Decay Curves of Charged Insulators

Figure 7 shows a number of total yield decay curves as a function of beam energy, representing the rate at which the sample exponentially approaches a (quasi-) steady state with successive pulses. Measurements in Figures 7a-d and 7e were taken for 8 μm and 25 μm thick polyimide Kapton H^{TM} samples. Data in Figure 7f were taken for the anodized aluminum sample. Measurements were made using a pulsed (~5 μsec), low current beam (~10-30 nA) focused on a sample area of ~1 mm^2 that is delivered pulses containing ~10^6 electrons/mm^2. Based on the data presented in Figure 4a, for Kapton that E_1~(30±10) eV, E_2~(962±25) eV, and E_{max}~(195±10) eV [3].
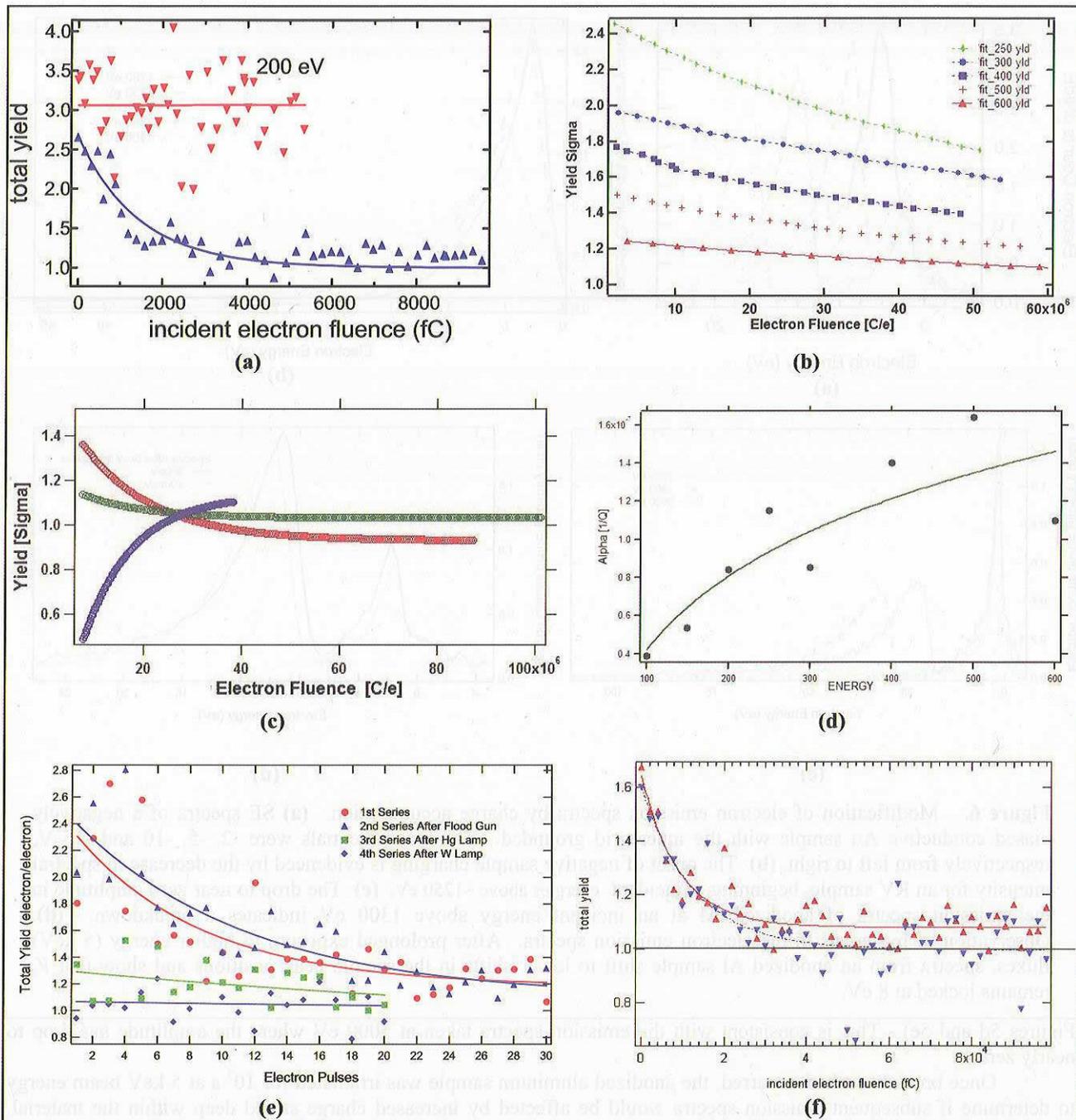
Figure 7.   Decay curves for insulators. Decay curves are for Kapton on Al samples, except as noted. **(a)** The evolution of the total yield as a function of pulsed incident electron fluence—and internal charge accumulation— at 200 eV between E_1 and E_2. Successive symbols are for consecutive pulses with (▼) and without (▲) charge neutralization with low energy electron flooding between pulses. Fits are for exponential decay of the total yields to (quasi-)steady state values based on Eq. 15 [3]. **(b)** Additional decay curves at increasing incident energies in the regime of $E_1 < E_0 < E_2$. **(c)** Decay cures for incident energies of 600 eV, 900 eV and 1200 eV, that is $E_1 < E_0 < E_2$, $E_0 \approx E_2$, and $E_0 > E_2$, respectively. Note that the crossover energy is about 965 eV. **(d)** Dependance of the charge decay constant $\alpha(Eo)$ on incident energy. The fit is proportional to a 0.5 power law. **(e)** Tests of the effectiveness of neutralization using an electron flood gun, UV light, and visible light neutralization for repeated electron pulsed yields at 500 eV. Decay curves are for the anodized aluminum sample. Fits are for exponential decay of the total yields based on Eq. 15 [3]. **(f)** Test of the effectiveness of thermal annealing of charge from a Kapton on Au sample. The red curve (▲) [blue curve (▼)] was done after moderate exposure to charges from beams in the energy range of 200 eV to 1000 eV below E_2 followed by a several minute exposure to the electron flood gun and a UV deuterium discharge lamp without [with]thermal annealing.

Figure 7a shows the evolution of the total yield as a function of pulsed incident electron fluence—and internal charge accumulation—at 200 eV between E_1 and E_2. Successive symbols are for consecutive pulses with ($\blacktriangledown$) and without ($\blacktriangle$) charge neutralization with low energy electron flooding between pulses. Similar curves at additional energies are found in [3]. The decay for $E_1<E_o<E_2$ occurred for small incident charges, since positive surface potentials quickly re-attracted a significant portion of the SE spectrum (see Figure 3c), an effect that was largely neutralized with low energy electron flooding. Between the crossover energies, the total yield without flooding asymptotically approaches unity exhibiting a decrease in total yield of >2.5 after only 2-5 pC/mm² of incident charge. Fits shown are based on the empirical model for exponential decay of the total yields to (quasi-)steady state values using Eq. 15. Fits using the emission spectra model of Eq. 14 are currently being studied.

Figure 7b shows similar decay curves for increasing energies from 250 eV to 600 eV, still in the regime of positive charging with $\sigma>1$ and $E_1<E_o<E_2$. The initial yield decreased with increasing incident energy, consistent with the uncharged yield curve in Figure 4a. The decay curves all decayed approximately exponentially towards unity, with the decay rate increasing with increasing incident energy. Figure 7c shows the evolution of the total yield as a function of incident charge—and internal charge accumulation—for incident energies of 600 eV, 900 eV and 1200 eV, that is for $E_1<E_o<E_2$, $E_o \approx E_2$, and $E_o>E_2$, respectively. Below E_2 the red curve exhibits an approximately exponential decrease to an asymptotic limit of unity. At slightly below E_2, the exponential decrease is still positive, but has a substantially smaller initial value. At $E_0=E_2$, the yield curve is expected to be unity for all fluences. Above E_2, the yield approaches an asymptotic limit of unity from below, increasing approximately exponentially.

Figure 7d shows the total yield decay constant, α, determined from fits to Eq. ?15, as a function of E_o [5]. The decay constant decreased with increasing E_0 up to $E_0=E_2$. This occurred for small incident charges, since positive surface potentials quickly re-attracted a significant portion of the SE spectrum (see figure above)—an effect that was largely neutralized with low energy electron flooding. The fit in Figure 7d shows that $\alpha(E_o)$ is approximately proportional to $E_o^{0.5}$. Beyond E_2, the decay constant remained small, but slightly positive as total yields and sample charge slowly approach their steady state values. This decrease of the charging rates for yields beyond E_2 resulted from the growing negative charge distribution that diminished the landing energy of the incident electrons [11], the so-called slow negative charging mechanism; the increased total yields at lower landing energies further reduced negative charge accumulation and lowered the rate.

To further explore the rates of sample charging as well as the effectiveness of the various neutralization methods, pulsed yields were taken repeatedly at a constant energy of E_{beam}=500 eV (using single 5 μs, 40-60 nA impulses) without any neutralization between incident electron pulses for an anodized aluminum sample. After the initial sequence (20-30 pulses were used in each sequence) of yield measurements, the electron flood gun was turned on for five minutes to test its discharging effectiveness [3]. Then, a second pulsing sequence was repeated. Next, the sample was irradiated with a mercury gas lamp for 15 minutes, and a third yield sequence was taken. Finally, the sample was irradiated with the tungsten filament lamp for 15 minutes, and a fourth pulsing sequence was taken. As can be seen from Figure 7e, for the initial pulsing sequence ($\bullet$), the total electron yield decayed asymptotically towards unity (steady state condition) with repeated pulsing, consistent with the flattening of yield data in Figures 7a and 7b. Fits shown are based on the empirical model for exponential decay of the total yields to (quasi-)steady state values using Eq. 15. In the second yield sequence (after flooding, ($\blacktriangle$)) the total yield was restored to its original uncharged value (within the error), and then once again declined at roughly the same charging rate towards unity. In the third ($\blacksquare$) and fourth sequence ($\blacklozenge$), it was observed that the mercury lamp was only partially effective in neutralizing the sample, while the tungsten lamp had almost no effect on the yield values. These results showed that in the energy regime between the crossover energies, the flood gun was very effective in neutralizing positive surface potentials, providing a way to measure repeatable electron yields. However, UV and visible light irradiation in this energy regime were not as effective, but still provide methods for negative-charge neutralization for beam energies beyond the second crossover energy[44].

Neutralization of the Kapton sample using both the low energy electron flood gun and a deuterium discharge lamp is shown in Figure 7f. The neutralization is largely effective, but a residual charge is observed. A fit to the decay curve based on Eq. 15 with an added asymptotic residual charge constant term, found a residual yield of ~8% above unity with a decay constant of (1.1 ± 0.1) pC⁻¹. Similar magnitudes of residual charges were observed for many other Kapton decay curves. The other decay curve was take immediately after the sample had been annealed at 50-70 °C for several hours. In this case, the asymptotic yield was 1.00 ± 0.02 with a decay constant of (0.78 ± 0.05) pC⁻¹. The thermal annealing is believed to have dissipated the residual charge, since the conductivity of insulating polymers is know to increase exponentially with temperature proportional to a Boltzmann factor involving the activation energy of hopping conductivity.

Conclusion

The studies described in this paper have demonstrated that pulsed electron methods provide an effective way to measure electron emission properties of uncharged insulators. They have also been shown to provide a sensitive tool to

explore the effects of accumulated charge from incident electron beams on the electron emission properties of insulators. The effect of internal charge accumulation has been quantitatively observed on (i) the secondary, backscattered and total yields and (ii) the position and magnitude of the emission spectra peaks. Distinct behavior has been observed in decay curves above and below the crossover energies, due to the sign of the net charge. Indeed, electron emission properties have been shown to be very sensitive to charge accumulation, showing pronounced effects after <50 pC/cm^2 of incident charge. Partially effective means have also been developed and characterized to neutralize charge built up within insulators.

Extensions to existing semi-empirical models for the yield curves and secondary electron emission spectra have been extended in simple ways to provide some initial description of the charge dependence of total, secondary and backscattered yield curves and of electron emission spectra; qualitative agreement is found for a wide array of measured effects. A simple model predicts the behavior of decay curves above and below crossover energies. These models are in qualitative agreement with measurements. The charge decay constant in the phenomenological model for the decay curves has been found to have incident energy dependence.

Acknowledgements

References

[1] J.R. Dennison, C.D. Thomson, J. Kite, V. Zavyalov, J. Corbridge, "Materials Characterization at USU: Facilities and Knowledgebase of Electronic Properties Applicable to Spacecraft Materials," Proc. 8th Spacecraft Charging Tech. Conf., (Huntsville, AL, USA), 2004.

[2] Nickles, N. E., The Role of Bandgap in the Secondary Electron Emission of Small Bandgap Semiconductors: Studies of Graphitic Carbon, Ph.D. Dissertation, Utah State University, 2002.

[3] C.D. Thompson, "Measurements of Secondary Electron Emission Properties of Insulators," Ph.D. dissertation, Utah State University, Logan, UT, 2004.

[4] JR Dennison, C. D. Thomson, and Alec Sim, "The effect of low energy electron and UV/VIS radiation aging on the electron emission properties and breakdown of thin-film dielectrics," Proceedings of the 8th IEEE Dielectrics and Electrical Insulation Society (DEIS) International Conference on Solid Dielectrics (ICSD), 967-971, (IEEE, Piscataway, NJ, 2004).

[5] Alec Sim, Instrumentation and Measurements for Electron Emission from Charged Insulators," MS Thesis; April, 2005.

[6] Sébastien Clerc J.R. Dennison and Clint Thomson, « Importance of Accurate Computation of Secondary Electron Emission for Modeling Spacecraft Charging," Proceedings of the 9th Spacecraft Charging Technology Conference, (EPOCHAL TSUKUBA, TSUKUBA, April 4-8, 2005).

[7] Dionne, G. F., "Effects of secondary electron scattering on secondary emission yield curves," J. Appl. Phys. 44 (12), 5361-5364 (1973).

[8] Chung, M. S., and T. E. Everhart, "Simple calculation of energy distribution of low-energy secondary electrons emitted from metals under electron bombardment," J. Appl. Phys. 45 (2), 707-709 (1974).

[9] Alig, R. C., and S. Bloom, "Secondary electron escape probabilities," J. Appl. Phys. 49 (6), 3476-3480 (1978).

[10] N. Nickles, R.E. Davies, J.R. Dennison, "Applications of Secondary Electron Energy- and Angular-Distributions to Spacecraft Charging," Proc. of the 8th Spacecraft Charging Tech. Conf., (AFRL Sc. Center, Hanscom AFB, MA, USA), 2000.

[11] L. Reimer, Scanning Electron Microscopy. Physics of Image Formation and Microanalysis, New York, USA: Springer-Verlag, pp. 119-121, 1985.

[12] Thomson, C. D., V. Zavyalov, J. R. Dennison, and J. Corbridge, "Electron emission properties of insulator materials pertinent to the international space station," Proceedings of the 8th Spacecraft Charging Technology Conference, Huntsville, AL, (2003a).

13] Akkerman A., and E. Akkerman, "Characteristics of electron inelastic interactions in organic compounds and water over the energy range 20–10000 eV," J. Appl. Phys. 86 (10), 5809-5816 (1999).

[14] X. Meyza, D. Goeuriot, C. Guerret-Piecout, D. Treheux, H.-J. Fitting, "Secondary Electron Emission and Self-consistent Charge Transport and Storage in Bulk Insulators: Application to Alumina," J. Appl. Phys., vol. 94, pp. 5384-5392, 2003.

[15] Grais, K. I., and A. M. Bastawros, "A study of secondary electron emission in insulators and semiconductors," J. Appl. Phys. 53, 5239-5242 (1982).

[16] Corbridge, J, J. R. Dennison, and N. Nickles, "Effects of bandgap on secondary electron emission for graphitic carbon semiconductors," American Physical Society Annual March Meeting, Austin, TX (2003).

[17] J. Cazaux, "Some considerations on the secondary electron emission δ, form e⁻ irradiated insulators," *J. Appl. Phys.*, vol. 85, no. 2, pp. 1137-1147, 1999.

[18] Sternglass, E. J., "Secondary electron emission and atomic shell structure," Phys. Rev. 80, 925-926 (1950); Sternglass, E. J., *An Experimental Investigation of Electron Back-Scattered and Secondary Electron Emission From Solids*, Ph.D. Dissertation, Cornell University, 1953.

[19] Young, J. R., "Penetration of electrons and ions in aluminum," J. Appl. Phys. 27 (1), 1-4 (1956).

[20] J.R. Dennison, A.R. Frederickson and Prasanna Swaminathan, "Charge Storage, Conductivity and Charge Profiles of Insulators As Related to Spacecraft Charging," *Proceedings of the 8th Spacecraft Charging Technology Conference*, (NASA Marshall Space Flight Center, Huntsville, Al, October 2003), 15 pp.

[21] A. Melchinger, S. Hofmann, "Dynamic double layer model: Description of time dependent charging phenomena in insulators under electron beam irradiation," *J. Appl. Phys.* vol. 78, pp. 6224-32, 2003.

[22] Cazaux, J., private communications, 2005.

[23] Cazaux, J., K. H. Kim, O. Jbara, and G. Salace, "Charging effects of MgO under electron bombardment and nonohmic behavior of the induced specimen current," J. Appl. Phys. 70 (2), 960-965 (1991).

[24] Cazeaux, J., "Charging in Scanning Electron Microscopy 'from Inside and Outside'," Scanning, 26, 2004.

[25] Miyake, H., Y. Tanaka, and T. Takada, "Characteristic of charge accumulation in glass materials under electron beam irradiation," Proceedings of the 8th Spacecraft Charging Technology Conference, Huntsville, AL, (2003).

[26] Osawa, N., S. Takahashi, Y. Tanaka, T. Takada, R. Watanabe, N. Tomita, V. Griseri, L. Levy, and C. Laurent, "Measurement of bulk charge in dielectric materials irradiated by electron beam in vacuum environment," Proceedings of the 8th Spacecraft Charging Technology Conference, Huntsville, AL, (2003).

[27] Usui, Y., T. Sakai, M. Ishikawa, T. Isono, Y. Tanaka, T. Takada, R. Watanabe, N. Tomita, and Y. Murooka, "Measurement of charge distribution in electron beam irradiated PMMA using electro-optical effect," Proceedings of the 8th Spacecraft Charging Technology Conference, Huntsville, AL, (2003).

[28] Tatsuo Takada, "Pulse Acoustic Technology for Measurement of Charge Distribution in Dielectric Materials for Spacecraft," *Proceedings of the 9th Spacecraft Charging Technology Conference*, (EPOCHAL TSUKUBA, TSUKUBA, April 4-8, 2005).

[29] Virginie Griseri, « Space Charge Detection and Behaviour Analysis in Electron Irradiated Polymers," *Proceedings of the 9th Spacecraft Charging Technology Conference*, (EPOCHAL TSUKUBA, TSUKUBA, April 4-8, 2005).

[30] Fuyuko Fukuyoshi, "Observation of Internal Charge Behavior in Electron Beam Irradiated Polymers Using Acoustic Method," *Proceedings of the 9th Spacecraft Charging Technology Conference*, (EPOCHAL TSUKUBA, TSUKUBA, April 4-8, 2005).

[31] JR Dennison, W.-Y. Chang, Neal Nickles, Jason Kite, and C.D. Thomson, *Final Report Part 1: Instrumentation, Methods and Analysis*, NASA Space Environments and Effects Program Grant, "Electronic Properties of Materials with Application to Spacecraft Charging," In preparation.

[32] Davies, R. E., *Measurement of Angle-resolved Secondary Electron Spectra*, PhD Dissertation, Utah State University, 1999.

[33] Chang, W. Y, J. R. Dennison, J. Kite, and R. E. Davies, "Effects of evolving surface contamination on spacecraft charging," Proceedings of the 38th American Institute of Aeronautics and Astronomics Meeting on Aerospace Sciences, Reno, NV (2000b).

[34] C.D. Thompson, V. Zavyalov, J.R. Dennison, J. Corbridge, "Electron Emission Properties of Insulator Materials Pertinent to the International Space Station," Proc. of the 8th Spacecraft Charging Tech. Conf., (Huntsville, AL, USA), 2004.

[35] C.D. Thomson, V. Zavyalov, J.R. Dennison, "Instrumentation for studies of electron emission and charging from insulators," Proc. of the 8th Spacecraft Charging Tech. Conf., (Huntsville, AL, USA), 2004.

[36] T. Schneider, NASA Marshall Space Flight Center, Materials, Processes, and Manufacturing Department, (private communications), 2003.

[37] Dennison, J. R., C. D. Thomson, and J. Corbridge, "Electronic properties of ISS materials," Boeing Company Final Report, Contract No. M/C H014-B419, 2003c (Available from J. R. Dennison at PHYSJRD@cc.usu.edu).

[38] Dennison, J. R., W. Y. Chang, N. Nickles, J. Kite, C. D. Thomson, J. Corbridge, and C. Ellsworth, "Final report part III: materials reports," NASA Space Environments and Effects Program Grant, "Electronic Properties of Materials with Application to Spacecraft Charging," Available in electronic format through NASA SEE as part of the SEE Charge Collector Knowledgebase (2002).

[39] A.R. Frederickson, "Radiation Induced Electrical Current and Voltage in Dielectric Structures," Phys. Sc. Res. Papers No. 613, AFCRL-TR-74-0582, Air Force Cambridge Res. Labs, (Hanscom AFB, MA), 1974.

[40] A. R. Frederickson, "Radiation induced voltage on spacecraft internal surfaces," *IEEE Trans. Nuclear Science*, vol. 40, no. 6, pp. 1547-1553, Dec. 1993.

[41] Liehr, H., P. A. Thiry, J. J. Pireaux, and R. Caudano, "Characterization of insulators by high-resolution electron-energy-loss spectroscopy: Application of a surface-potential stabilization technique," Phys. Rev. B **33** (8), 5682-5697 (1986).

[42] J.R. Dennison, Prasanna Swaminathan, Randy Jost, Jerilyn Brunson, Nelson Green and A. Robb Frederickson, "Proposed Modifications to Engineering Design Guidelines Related to Resistivity Measurements and Spacecraft Charging," *Proceedings of the 9ᵗʰ Spacecraft Charging Technology Conference,* (EPOCHAL TSUKUBA, TSUKUBA, April 4-8, 2005).

[43] Prasanna Swaminathan , "Measurement of Charge Storage Decay Time and Resistivty of Spacecraft Insulators," MS Thesis; August, 2004.

[44] L. Levy, D. Sarrail, and J. M. Siguier, "Conductivity and secondary electron emission properties of dielectrics as required by NASCAP," *Third European Symposium on Spacecraft Materials in Space Environment*, pp. 113-123, 1985.

[45] Dennison, J. R., J. Kite, W. Y. Chang, and R. E. Davies, "Absolute and differential spacecraft charging as a result of evolving surface contamination," Proceedings of the 7ᵗʰ Spacecraft Charging Technology Conference, Noordwijk, Netherlands (2001).